A Multistate Single-Connection Calibration for Microwave-Microfluidics

Xiao Ma, *Student Member, IEEE,* Nathan D. Orloff, Charles A. E. Little, Christian J. Long, Isaac E. Hanemann, Song Liu, Jordi Mateu, *Senior Member, IEEE*, James C. Booth, and James C.M. Hwang, *Life Fellow, IEEE*

Abstract—**With emerging medical, chemical, and biological applications of microwave-microfluidic devices, many researchers desire a fast and accurate calibration that can be achieved in a single connection. However, traditional on-wafer or coaxial calibrations require measurements of several different artifacts to the data prior to measuring the microwave-microfluidic device. Ideally, a single artifact would be able to present different impedance states to correct the vector network analyzer data, minimizing drift and eliminating artifact-to-artifact connection errors. Here, we developed a multistate single-connection calibration that used a coplanar waveguide loaded with a microfluidic channel. We then used measurements of the uncorrected scattering parameters of the coplanar waveguide with the channel empty, filled with deionized water, and filled with 30 w% (30 grams per liter) of saline to construct an eight-term error model and switch-term correction. After correction, the residuals between measured scattering parameters and with literature-based finite-element simulations were below -40 dB from 100 MHz to 110 GHz. This multistate single-connection calibration is compatible with both wafer-probed and connectorized microwave-microfluidic devices for accurate impedance spectroscopy and materials characterization without the need for multiple device measurements.**

Index Terms—**Calibration, microwave, microfluidics, vector network analyzer, scattering parameters.**

X. Ma and J. C. M. Hwang are with the Department of Electrical and Computer Engineering, Lehigh University, Bethlehem, PA 18015 USA (e-mail: xim214@lehigh.edu).

N. D. Orloff, C. J. Long, I. E. Hanemann and J. C. Booth are with the National Institute of Standards and Technology, Boulder, CO 80305 USA (e-mail: orloff@nist.gov).

C. A. E. Little are with the National Institute of Standards and Technology, Boulder, CO 80305 USA and University of Colorado Boulder, Boulder, CO 80309 USA.

S. Liu was with the National Institute of Standards and Technology, Boulder, CO 80305 USA and was with the Departement Elektrotechniek–Telecommunications and Microwaves, Katholieke Universiteit Leuven, 3001 Leuven, Belgium.

J. Mateu are with Dep. Signal Theory and Communications, Universitat Politecnica de Catalunya (UPC), 08034, Barcelona Spain and Centre Tecnologic de Telecomunicacions de Catalunya (CTTC), 08860, Castelldefels, Spain.

I. INTRODUCTION

MICROWAVE-MICROFLUDIC devices integrate microwave circuits with microfluidics for quantitative electrical measurement of fluids [1]–[5]. This emerging field has the potential to advance industrial applications of impedance spectroscopy, including point-of-care diagnostics and quality assurance for pharmaceutical and chemical manufacturers [4], [6]. For these commercial applications to be realized, it is important to accurately and quickly correct the electrical measurements of microwave-microfluidic devices for the attenuation and phase shift of the measurement leads and the standing waves between the fluid-under-test and the vector network analyzer (VNA) [7]–[11].

Due to its basis in circuit theory, the on-wafer multiline thru-reflect-line (TRL) calibration algorithm [12] is the most accurate VNA calibration algorithm. However, like other calibration algorithms—e.g., load-reflect-match [13], [14], series-resistor [15], and short-open-load-thru [16], etc.—the multiline TRL calibration [17], [18] requires more than one calibration artifact. For on-wafer measurements, this requirement means one must move the wafer probes to contact different artifacts. For connectorized measurements, this problem is even worse, because the disconnect between artifacts can occur behind the reference plane of the microfluidic channel. Moving the probes or exchanging calibration artifacts has been shown to introduce connection errors between different measurements of the scattering (S-) parameters [19], which ultimately increases the measurement uncertainty [20]. Increasing the measurement uncertainty has the potential to overwhelm sample-to-sample differences or result in false-positive statistics, which may limit the motivating applications for microwave-microfluidics. Hence, a fast and accurate calibration algorithm is needed; one that can be done on the microwave-microfluidic device itself [21], [22] in a single connection without separate calibration artifacts. Such a multistate single-connection calibration would facilitate testing of sources of uncertainty that limit the signal-to-noise ratio, the measurement drift of the VNA, and even the drift of the fluid sample itself.

Our approach for calibrating microwave-microfluidic devices is to use fluids of known electrical properties to access different impedance states, and then use those artifacts to build an error model (Fig. 1) as in the series-resistor calibration
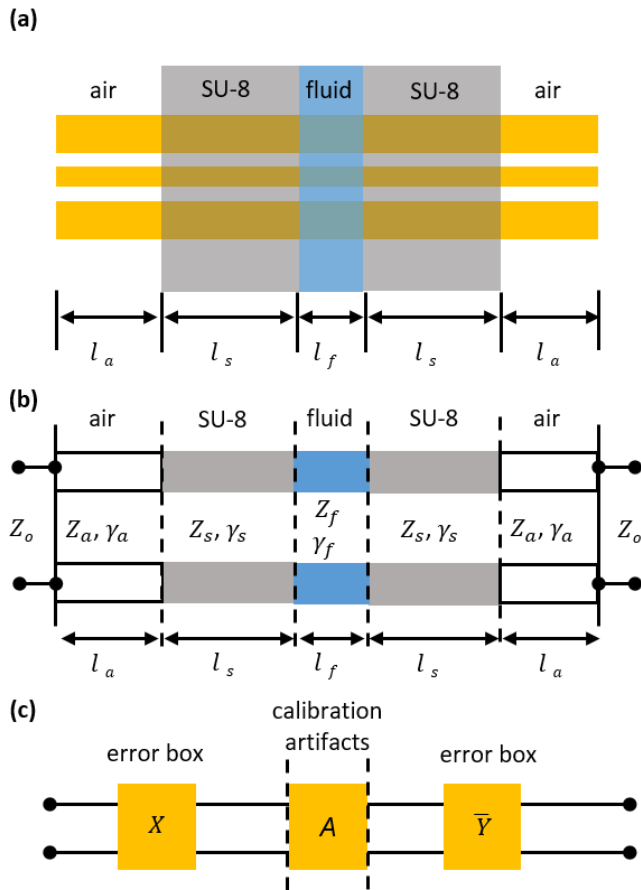
Fig. 1. Diagram of the microwave-microfluidic device. (a) Schematic representation of different regions that are modeled. (b) Transmission-line model where Z_o is the system impedance, and Z, γ and l are the characteristic impedance, propagation constant, and length of regions under air, SU-8 and fluid as denoted by subscripts "a", "s" and "f", respectively. The substrate for all regions is quartz and the microfluidic channel side-walls are SU-8. (c) Measurement model for VNA without coupling between two ports. Error boxes X and $\overline{Y}$ are matrices to be determined by the calibration artifacts A in the calibration procedure.

algorithm [15]. In lieu of the series resistor, we developed an algorithm for correcting the S-parameters of a microwave-microfluidic transmission line that uses known fluids as the calibration artifacts. Here, we show that a microfluidic channel filled with different known fluids enables a multistate single-connection calibration with the reference plane directly adjacent to the channel. This proposed calibration requires only two known fluids to correct the S-parameters of a microwave-microfluidic device with an unknown fluid. The single-connection calibration results in S-parameter errors like those obtained with a microfluidic-multiline TRL calibration, which uses fluid-loaded transmission lines that have different lengths. Compared to the microfluidic-multiline TRL calibration, the multistate single-connection calibration greatly reduces measurement time and simplifies impedance spectroscopy.

In the following, Section II-A discusses a multistate single-connection calibration based on the measurement of a microwave-microfluidic device with known fluids (Fig. 2).
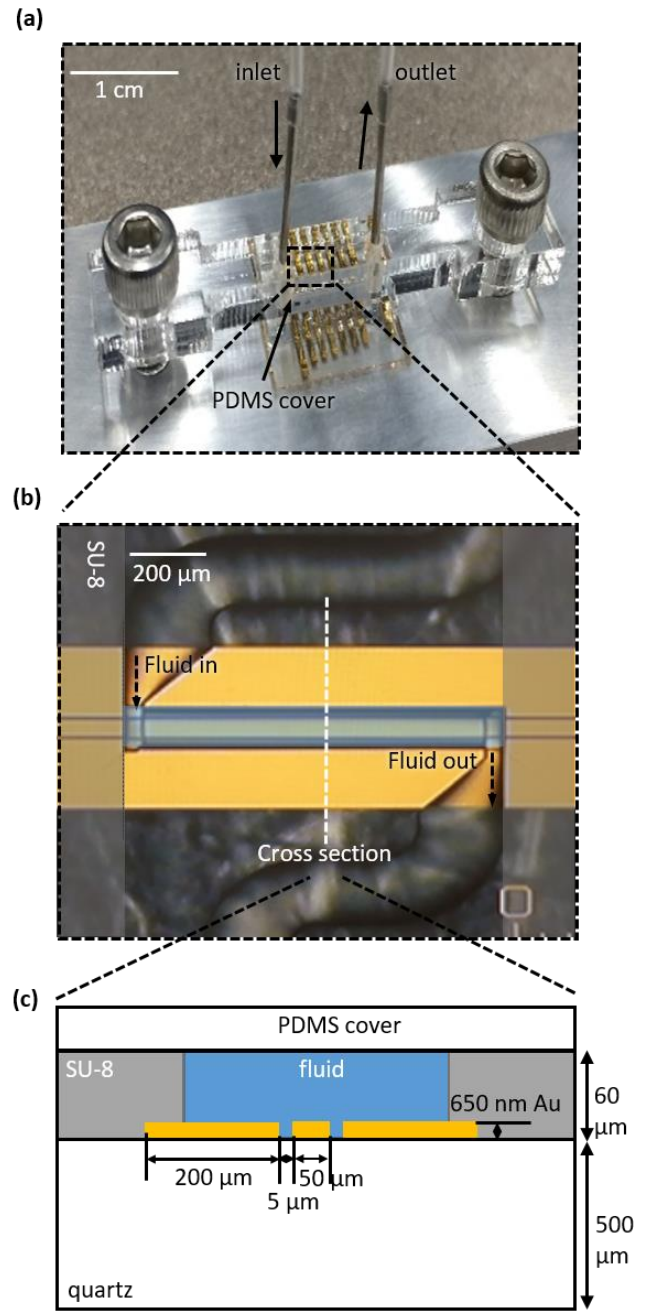

Fig. 2. Top and cross-section views of the microwave-microfluidic device. (a) Photograph showing the device under test consisting of a gold coplanar waveguide (CPW) under a microfluidic chamber formed by a PDMS cover. (b) Micrograph showing microfluidic channel confined on the left and right by SU-8 walls. Microfluidic device for measuring S-parameters of a fluid in a single connect. The SU-8 (grey regions) formed the channel wall and confined the fluid to the fluid channel (light blue region), where the fluid flowed from left to the right in the measurement. (c) Cross-sectional dimensions of the CPW in the channel region, which is 850 μm long and 0.65 μm thick with the widths of center electrode, electrode spacing, and ground electrodes being 50 μm, 5 μm and 200 μm.

Section II-B describes the use of the multistate single-connection calibration to extract the error boxes that de-embed the microfluidic channel. The design and fabrication of the microwave-microfluidic device is introduced in Section III. We then compare and validate the multistate

single-connection calibration with a co-fabricated microfluidic-multiline TRL calibration and finite-element simulation in Section IV-A and Section IV-B, respectively. Section IV-C provides data for different numbers of known fluid artifacts. Finally, we summarize our findings in Section V and offer a perspective on how the multistate single-connection calibration can be applied.

II. THEORY

A. Artifacts

Like our previous work [23], this microwave-microfluidic device had five regions (Fig. 1(a)), which are modeled as uniform distributed transmission-line segments. We labeled each segment per the material above: air, SU-8, and fluid. As shown in Fig. 1(b), the microwave-microfluidic device consisted of two air segments, two SU-8 segments, and a fluid segment. The air segments had length l_a, characteristic impedance Z_a, and propagation constant γ_a; the SU-8 segments had length l_s, characteristic impedance Z_s, and propagation constant γ_s; and, the fluid segment had length l_f, characteristic impedance Z_f, and propagation constant γ_f. The reference impedance for the model (Fig. 1(b)) was Z_o. The models for the calibration artifacts A (Fig. 1(c)) were simply the microwave-microfluidic device with different known fluids.

The calibration artifact models (A) require γ_f, Z_f, l_f, transmission (T-) matrix model of the transmission line, and impedance transformers [24]. From the telegrapher's equations [25], we wrote γ_f, and Z_f as

$$\gamma_f = \sqrt{(R_f + i\omega L_f)(G_f + i\omega C_f)}, \text{ and} \tag{1}$$

$$Z_f = \sqrt{\frac{(R_f + i\omega L_f)}{(G_f + i\omega C_f)}}, \tag{2}$$

where R_f, L_f, C_f, and G_f were the distributed resistance, inductance, capacitance and conductance per unit length of the transmission line loaded by the fluid. The parameters R_f, L_f, C_f, and G_f are dependent on frequency, which we omitted for clarity.

There were several approaches to obtaining R_f, L_f, C_f, and G_f for the known fluid samples, including finite-element simulation [23], direct measurement [23], and analytical calculation [26]. If the materials used to fabricate the microwave-microfluidic transmission lines (including the fluid) are nonmagnetic, then R_f and L_f depend solely on the metallic conductors [27]. In this nonmagnetic case, both finite-element simulations and analytical calculations [23], [28] could be used to obtain R_f and L_f from the cross-sectional dimensions of the transmission line. Then, either finite-element simulation or conformal mapping can be used to obtain geometrical factors, m and n, that relate C_f and G_f to the complex permittivity of the fluid. The dielectric constant extraction method for different fluids at the full frequency band

from 100 MHz to 110 GHz can be found in [23]. For a known fluid of complex permittivity $\tilde{\epsilon}_f$, the C_f, and G_f are

$$G_f + i\omega C_f = \frac{\tilde{\epsilon}_f}{m} + \frac{\tilde{\epsilon}_q}{n}, \tag{3}$$

where $\tilde{\epsilon}_q$ is the complex permittivity of the substrate. Note that (3) assumes that the contribution of the fluid is in parallel with that of the substrate, which is only true for a CPW on a dielectric with a uniform fluid on top covering both gaps.

After computing R_f, L_f, C_f, and G_f for the known fluid artifacts, we obtained γ_f and inserted it into the T-matrix model of the transmission line segment of length l_f:

$$T^{l_f} = \begin{bmatrix} e^{-\gamma_f l_f} & 0 \\ 0 & e^{\gamma_f l_f} \end{bmatrix}. \tag{4}$$

Then Z_f could be used to construct the T-matrix model of the impedance transformer [24] that transitioned from Z_o to Z_f,

$$Q_{Z_f}^{Z_o} = \frac{1}{2Z_o} \left| \frac{Z_o}{Z_f} \right| \sqrt{\frac{Re(Z_f)}{Re(Z_o)}} \cdot \begin{bmatrix} Z_o + Z_f & Z_o - Z_f \\ Z_o - Z_f & Z_o + Z_f \end{bmatrix}. \tag{5}$$

$Q_{Z_o}^{Z_f}$ is the inverse of $Q_{Z_f}^{Z_o}$. We then multiplied the left and right sides of (4) by $Q_{Z_f}^{Z_o}$ and $Q_{Z_o}^{Z_f}$, respectively, to obtain the T-matrix model relative to Z_o as,

$$T_{Z_o, Z_f}^{l_f} = Q_{Z_f}^{Z_o} T^{l_f} Q_{Z_o}^{Z_f}. \tag{6}$$

In the next section, we develop the multistate single-connection calibration algorithm based on (6) and switch to a more conventional simplified notation, where $T_{Z_o, Z_f}^{l_f} = A$.

B. Algorithm

After we used (6) to form the T-matrices of different known fluid artifacts, we derived the multistate single-connection calibration algorithm that solved for the error boxes X and $\bar{Y}$ (Fig. 1(c)), which included everything between port 1 of the VNA to the fluid and from the fluid to port 2 of the VNA, respectively. In this case, any measurement (M) could be expressed as

$$M = XA\bar{Y}. \tag{7}$$

For an artifact A_a and measurement M_a, $\bar{Y}$ could be solved as

$$\bar{Y} = A_a^{-1} X^{-1} M_a. \tag{8}$$

Inserting (8) in (7), we derive

$$M = XA(A_a^{-1} X^{-1} M_a). \tag{9}$$

Following [15], we could either set X or Y to be reciprocal without losing the generality of the error model. We chose X to be reciprocal with form

$$X = r \begin{bmatrix} 1 & a \\ b & c \end{bmatrix}, \tag{10}$$

where $r = (c - ab)^{-\frac{1}{2}}$. This eliminated one unknown in X. We then solved for the unknown complex parameters a, b, and c by measuring another fluid artifact. Above (7)–(10) are all taken from [15].

At least two artifacts are required to solve (9) for the unknown complex parameters a, b, and c. We chose to use measurements of the microwave-microfluidic device filled with air (M_a), and deionized (DI) water (M_w). The corresponding models were A_a, and A_w for air and water, respectively. We inserted M_a, M_w A_a, and A_w into (9), which imposed four conditions on the a, b, and c. These conditions were

$$-[A_{21}^w(A_{11}^a)^{-1} + A_{22}^w(A_{21}^a)^{-1}]a + (M_wM_a^{-1})_{12}b =$$
$$A_{11}^w(A_{11}^a)^{-1} + A_{12}^w(A_{21}^a)^{-1} - (M_wM_a^{-1})_{11}. \tag{11}$$

$$[(M_wM_a^{-1})_{11} - A_{21}^w(A_{12}^a)^{-1} - A_{22}^w(A_{22}^a)^{-1}]a +$$
$$(M_wM_a^{-1})_{12}c = A_{11}^w(A_{12}^a)^{-1} + A_{12}^w(A_{22}^a)^{-1}. \tag{12}$$

$$[(M_wM_a^{-1})_{22} - A_{11}^w(A_{11}^a)^{-1} - A_{12}^w(A_{21}^a)^{-1}]b -$$
$$[A_{21}^w(A_{11}^a)^{-1} + A_{22}^w(A_{21}^a)^{-1}]c = -(M_wM_a^{-1})_{21}. \tag{13}$$

$$(M_wM_a^{-1})_{21}a -$$
$$[A_{11}^w(A_{12}^a)^{-1} + A_{12}^w(A_{22}^a)^{-1}]b + [(M_wM_a^{-1})_{22} -$$
$$A_{21}^w(A_{12}^a)^{-1} - A_{22}^w(A_{22}^a)^{-1}]c = 0. \tag{14}$$

where A_{ij} is a matrix element of A. Since (11)–(14) overdetermined a, b, and c, we used a least-squares algorithm [29] to obtain the complex values of a, b, and c.

Generally, the more artifacts included in the calibration, the more conditions there are on a, b, and c. Any two artifacts imposed four conditions on a, b, and c. Hence, n artifacts would impose $4 \times \frac{n(n-1)}{2}$ conditions on a, b, and c. This means that the number of conditions increases quadratically with the number of artifacts. We expect that increasing n would improve the worst-case error comparison to the microfluidic-multiline TRL calibration.

III. FABRICATION OF THE MICROWAVE-MICROFLUIDIC DEVICE

In this section, we discuss the fabrication of the microwave-microfluidic device, the microfluidic-multiline TRL test set, and a companion dry reference wafer with conventional on-wafer artifacts. All of them were co-fabricated to reduce the effect of fabrication tolerances. We chose quartz (fused silica) as the substrate for all the devices due to its low dielectric loss and homogenous dielectric constant. Devices were fabricated on a 76.5 mm diameter and 0.5 mm thick quartz wafer, and the dimensions of quartz and other layers were labeled in Fig. 2(c). A commercial stepper that used projection lithography was used to pattern each layer. The stepper had layer-to-layer alignment better than 250 nm [30].

Each wafer was fabricated in five layers for resistor, pads, conductors, SU-8, and polydimethylsiloxane (PDMS), respectively. The resistor, pad, and conductor layers were deposited by electron-beam evaporation and lifted off via a two-layer resist process [31]. First, we deposited a 1-nm Ti adhesion layer followed by 10 nm of PdAu for the resistor [32]. Next, a 10-nm Ti adhesion layer was deposited followed by 100 nm of Pd for the pads. Later, we deposited a 10-nm Ti adhesion layer followed by 650 nm of Au for the conductor. The CPW had a 50-μm-wide center conductor with 5-μm gaps from 200-μm-wide ground planes (Fig. 2(c)).

We added the microfluidics onto the wafer with the SU-8 [33] sidewalls and PDMS roof (Fig. 2). We first spin-coated the wafer with SU-8 to a thickness of 60 μm. Second, we patterned it with the stepper, using an exposure dose of 200 mJ /cm², a post-exposure-bake at 55 ℃ for 1 hour, and developed it to define the microfluidics. To remove crazing, we performed a post-develop bake to 150 ℃ for 5 min, then let it cool to room temperature on the hot plate. After the SU-8 layer, we diced the wafer into individual 12 mm × 12 mm dies. The PDMS layer was patterned following a procedure outlined in [34], which produced the PDMS layer's microfluidic channels. Finally, we placed the PDMS onto the SU-8 layer under a microscope and sealed the completed microwave-microfluidic with a clamp.

The completed microwave-microfluidic device (Fig. 2) had inlet and outlet for the microfluidic channels. The device consisted of a full microfluidic-multiline TRL test set with four transmission lines of lengths (0.5, 0.85, 1.55, 3.314) mm and a 0.25-mm offset short-circuit reflect. We selected the 0.85-mm line to demonstrate the multistate single-connection calibration (Fig. 2(b)). The companion dry reference wafer had identical conductor cross-sections to the microwave-microfluidic device. On this wafer, we fabricated a 10-μm series resistor, a 10-μm series capacitor, a short-circuit reflect, and seven bare CPW transmission lines with lengths (0.420, 1.000, 1.735, 3.135, 4.595, 7.615, 9.970) mm. Each lumped element artifacts had a 0.21 mm offset, which was half the length of the 0.42 mm thru.

IV. METHODOLOGY

A. Measurement

We measured the S-parameters of the microwave-microfluidic device, the microfluidic-multiline TRL test set, and the dry calibration artifacts on the companion reference wafer, using an intermediate frequency bandwidth of 50 Hz and a power level of -20 dBm for the Anritsu MS4647A VNA with extender heads. The small input power is used to ensure the extender heads were linear. However, one must take care when performing microwave-microfluidic measurements, as some fluids may absorb microwave energy. The measurement setup is probe based and the S-parameters were measured from 100 MHz to 110 GHz in 512 logarithmic steps. The measurements were performed on a temperature-controlled probe station at 28.5 ± 0.5 °C. The quality of the calibration is dependent on the temperature dependence of the
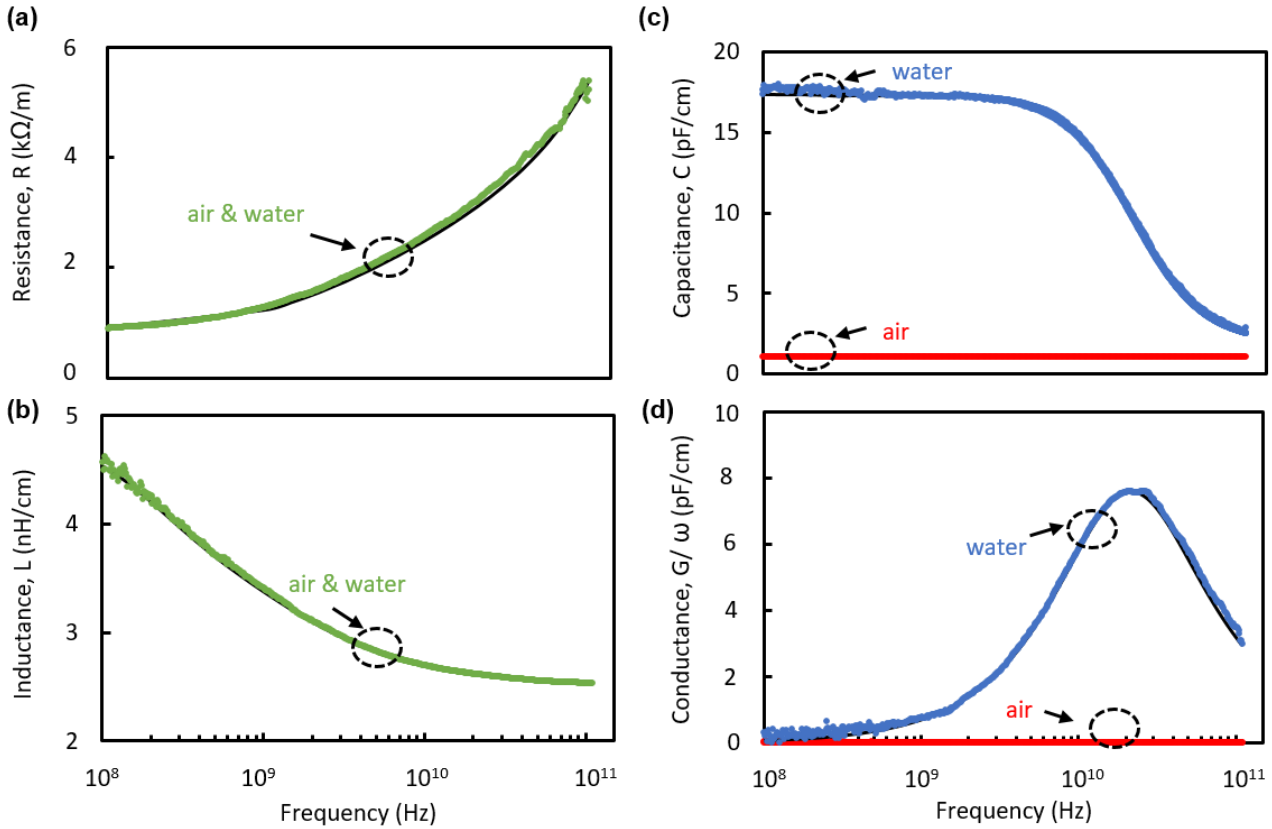
(a)

(b)

(c)

(d)

Fig. 3. Distributed resistance R (a), inductance L (b), capacitance C (c), and conductance G (d) for microwave-microfluidic coplanar waveguide under air or water. The finite-element simulated results are shown as solid lines while multiline thru-reflect-line (TRL) extracted results are shown in dotted lines. The finite-element simulations agreed with the multiline TRL measurements to within the measurement uncertainty.

microwave-microfluidic device, and the temperature sensitivity of the states. We tested the temperature dependence of our microwave-microfluidic device and its associated calibration by varying the temperature dependence of the model and recalculating the difference between microfluidic-multiline TRL and our approach. The result of this test proved that our microwave-microfluidic device was insensitive to deviations on the order of 1 °C. And 1 minute is also ample amount of time to assume thermal equilibrium between injected fluids and the probe station which we measured directly. After measuring the dry calibration artifacts on the companion reference wafer, we placed the microwave-microfluidic device onto the temperature-controlled probe station. Then the raw

S-parameters of the device were measured with the microfluidic channel filled with air, DI water, and (30 w% and 3 w%) saline solutions. We first flushed out the channels with air followed by DI water three times to make sure the channels were clean, and then injected new samples. Since the time to clean the channel is a function of the fluid flow rate and the total channel volume, it takes roughly 0.01 second to completely change fluids. A microfluidic switch could be used to automatically control and change artifacts during the calibration, which would reduce the time between measurements and minimized the effect of measurement drift along with the time.

B. Analysis

The analysis is divided into two parts: 1) the microfluidic-multiline TRL test set and 2) the microwave-microfluidic device. To analyze the S-parameters of the microfluidic-multiline TRL test set, we performed a two-tier calibration [18], which used the S-parameters of the multiline TRL calibration artifacts on the companion reference wafer to extract error boxes between the VNA and the probe tips. This first-tier calibration also extracted the propagation constant of the CPW without the microfluidics, which we assumed was equal to the microwave-microfluidic CPW with air in the channel. In this step, we also corrected the data for the
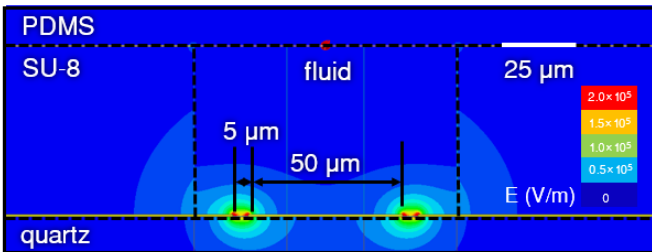
Fig. 4. Finite-element simulated electrical-field distribution across a water-filled channel of the microwave-microfluidic device. The electric-field is strongest in the coplanar waveguide gap.
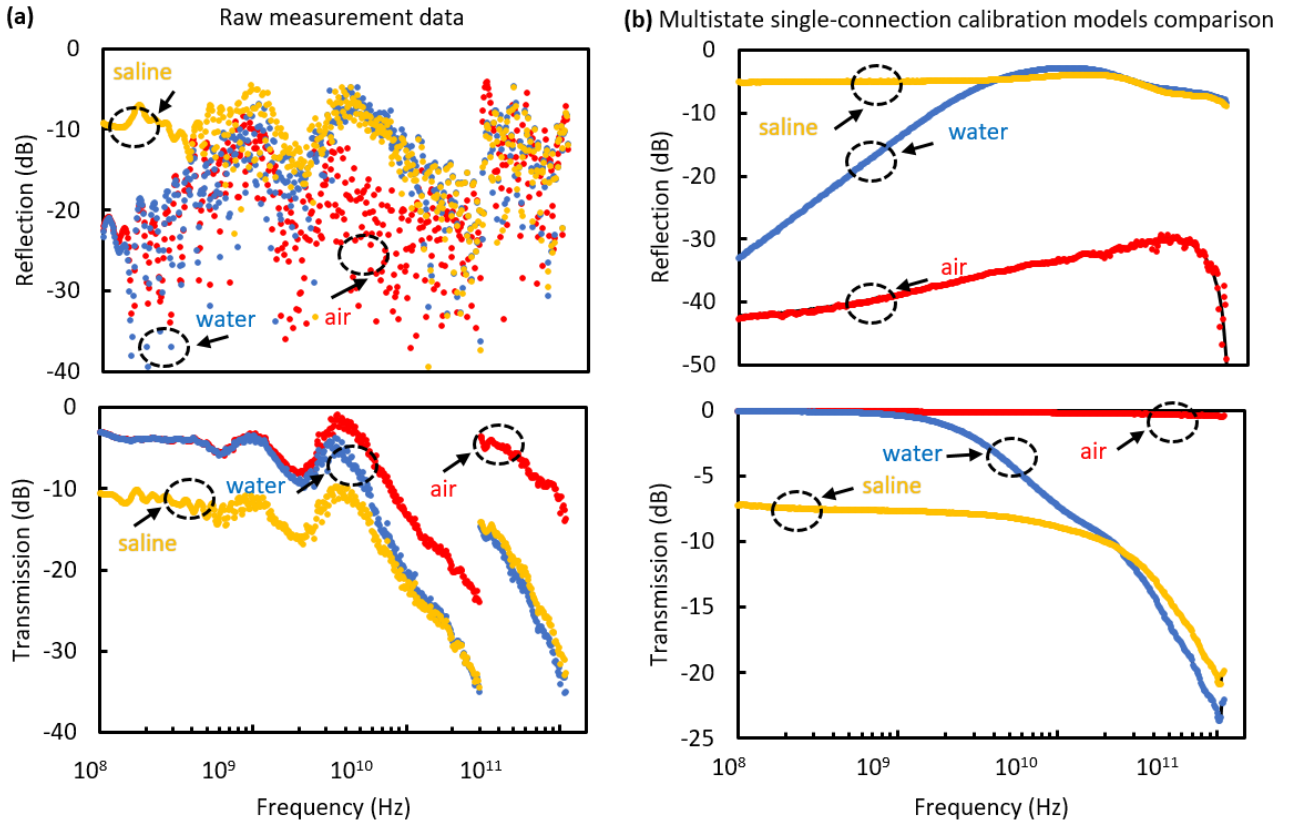
Fig. 5. Demonstration of the multistate single-connection calibration. (a) As-measured reflection and transmission coefficients from 100 MHz to 110 GHz for the microwave-microfluidic device filled with air (red triangles), water (blue squares) and 30 w% saline (yellow dots), respectively. (b) The models used to generate the multistate single-connection calibration (black lines) and microfluidic multiline thru-reflect-line (TRL) corrected results (dots). The models used to compute the multistate single-connection calibration agree with the microfluidic-multiline TRL results to within the measurement uncertainty.

switch terms [35]. Next, we transformed the reference impedance to 50 Ω using the resistor, and empirically computed the capacitance per unit length of the CPWs on the quartz substrate $\left(C_q = \frac{\bar{\epsilon}_q}{m} \because G_q \approx 0 \right)$ [23]. Having obtained C_q (air, Fig. 3(c) and (d)), we used the propagation constant to obtain R_f (Fig. 3(a)) and L_f (Fig. 3(b)). It is true that most the frequency dependence of loss is consistent with the classical skin effect, but the geometrical effects can also have a significant role for the CPW configuration [28], [36]. We then corrected the S-parameters of the microfluidic-multiline TRL test set to 50 Ω, and performed a second-tier calibration to obtain γ_f and the second-tier error boxes. And we calculated C_f and G_f from γ_f using R_f and L_f, which allowed us to transform the second-tier error boxes to 50 Ω. This enabled us to verify that the modeled values of C_f and G_f were consistent with the measurements and the literature [23]. Finally, we cascaded the first-tier error boxes with the second-tier error boxes to construct the total error boxes that extended from the microfluidic channel to the VNA in 50 Ω.

In addition to extracting R_f, L_f, C_f, and G_f from measured S-parameters, we calculated these parameters (solid lines, Fig. 3) for the water and air cases based on finite-element simulations of the microwave microfluidic device (Fig. 4), using the measured DC resistivity of gold (ρ = 2.57e^{-8} S/m), relative permittivity of substrate ($\epsilon_r = 3.83$) and literature

values for the permittivity of air and water (ε = 76.39, τ_1 = 7.39 ps, $\epsilon_2 = 5.75$, $\tau_2 = 0.9$ ps, $\epsilon_\infty = 4.6$) [37]. We optimized the mesh of the finite-element simulation with a 1 % convergence on the calculated admittance.

After confirming that the simulated R_f, L_f, C_f, and G_f agreed with the microfluidic-multiline TRL corrected result to within the measurement uncertainty, we used the finite-element simulations to construct S-parameter models of the microwave-microfluidic device filled with air (A_a), water (A_w), and 30 w% saline (A_s) based on (1)–(6). We then used these models and the measured raw S-parameters M_a, M_w, and M_s (Fig. 5(a)) in multistate single-connection calibration based on (11)–(14). Note that the discontinuity around 30 GHz in raw data is purely due to the specific VNA using extender heads, which give rise to this discontinuity. These multistate single-connection model A_a, A_w, and A_s (solid line, Fig. 5(b)) compared well with microfluidic-multiline TRL corrected results (circles, Fig. 5(b)). In both cases, the reference planes of both the microfluidic-multiline TRL calibration and the single connection calibration are at the planes of the interface between the SU-8 and fluid with a reference impedance of 50 Ω.

C. Validation

With three sets of error boxes from the microfluidic-multiline TRL calibration, consisting of multistate
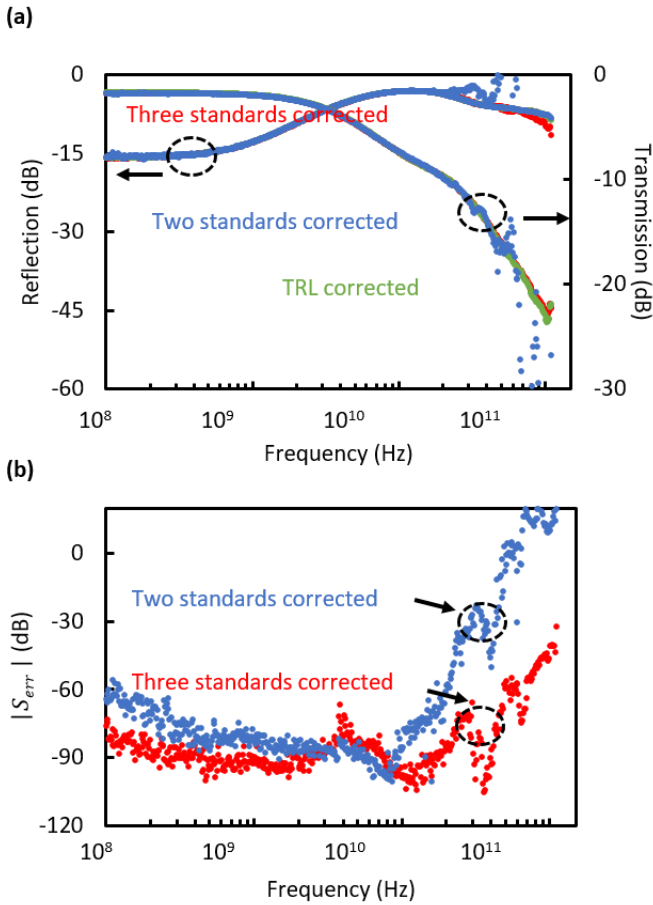
(a)

(b)

Fig. 6. Validation of the multistate single-connection calibration relative to finite-element simulations and microfluidic multiline thru-reflect-line (TRL). (a) Comparison and (b) error of reflection and transmission coefficients of the microwave-microfluidic device filled with 3 w% saline single- contact corrected with two (blue circles) or three artifacts (red squares) vs. multiline TRL corrected results (green triangles). This demonstrates that the multistate single connection calibration is consistent with microfluidic multiline TRL.

single-connection calibration with two known fluids (air, water), and multistate single-connection calibration with three artifacts (air, water, and 30 w% saline), respectively, we used each set of error boxes to correct the as-measured S-parameters of the microwave-microfluidic device filled with an "unknown" fluid (3 w% saline, in reality). The corrected S-parameters agreed with microfluidic-multiline TRL calibration (green triangles, Fig. 6(a)) and the multistate single-connection calibrations (two artifacts: blue circles; three artifacts: red squares). Both the reflection (left-axis, Fig. 6(a)) and transmission (right axis, Fig. 6(a)) agreed between calibration methods up to 20 GHz. Above 20 GHz, both reflection (left-axis, Fig. 6(a)) and transmission (right axis, Fig. 6(a)) deviated from the microfluidic-multiline TRL results. The deviation from microfluidic-multiline TRL results was much larger for the two artifact case (blue circles, Fig. 6(a)) compared to the three artifact case (red squares, Fig. 6(a)). For frequencies above 60 GHz, the three artifact case also disagreed with the microfluidic-multiline TRL result. We hypothesize that additional artifacts would place more constraints on a, b, and c in (11)–(14), which would further improve the agreement

between the multistate single-connection calibration and microfluidic-multiline TRL calibration. The method to extract permittivity of saline solution over such broad frequency bandwidth has been well studied in [38].

To better illustrate the difference between the corrected S-parameters, we calculated an error function (S_{err}, Fig. 6(b)),

$$|S_{err}| = \sqrt{\sum_{i,j=1}^{N=2}|S_{ij}^{SCC} - S_{ij}^{TRL}|^2}, \qquad (15)$$

where S_{ij}^{TRL} were microfluidic-multiline TRL corrected S-parameters and S_{ij}^{SCC} were multistate single-connection corrected S-parameters. This error function facilitates visualizing the difference between the two calibrations, as well as the effect of additional artifacts. As shown in Fig. 6(b), S_{err} was less than -60 dB below 20 GHz, but increased according to a power law above 20 GHz. Yet, even at 110 GHz, the S_{err} was less than -40 dB for the three artifacts case. (red circles, Fig. 6(b)).

V. CONCLUSION

In this paper, we established a multistate single-connection calibration algorithm and technique for microwave-microfluidic devices, providing an accurate calibration at the reference planes of the microfluidic channel to a reference impedance of our choosing for frequencies up to 110 GHz. We demonstrated the single-connection calibration algorithm with microwave-microfluidic devices filled with air, water, and 30 w% saline. We then used finite-element simulation and literature values to construct models that we validated with microfluidic-multiline TRL calibration. Next, we applied the single-connection calibration using two or three known fluids, and compared the results to microfluidic-multiline TRL calibration. With three artifacts, multistate single-connection calibration produced the least-square error from the microfluidic-multiline TRL calibration below −30 dB from 100 MHz to 110 GHz.

Future work will include an uncertainty analysis on the multistate single-connection calibration to clearly define the error and repeatability of the experiment and test microfluidic techniques to achieve variable states. Two key questions remain: 1) how different do the impedance states of the artifacts need to be; and 2) how increasing the number of states improves the calibration accuracy. In a word, we developed a multistate single-connection calibration algorithm that can be performed by simply measuring known fluids, which is essential for the commercialization of microwave-microfluidic devices. This calibration protocol could be easily extended to packaged devices by connectorizing the microwave microfluidics.

REFERENCES

[1] G. M. Whitesides, "The origins and the future of microfluidics," *Nature*, vol. 442, no. 7101, pp. 368–373, Jul. 2006.

[2] D. Mark, S. Haeberle, G. Roth, F. von Stetten, and R. Zengerle, "Microfluidic lab-on-a-chip platforms: requirements, characteristics and applications," *Chem. Soc. Rev.*, vol. 39, no. 3, pp. 1153–1182, 2010.

[3] D. Witters, K. Knez, F. Ceyssens, R. Puers, and J. Lammertyn, "Digital microfluidics-enabled single-molecule detection by printing and sealing single magnetic beads in femtoliter droplets," *Lab. Chip*, vol. 13, no. 11, pp. 2047–2054, 2013.

[4] A. Manz, N. Graber, and H. M. Widmer, "Miniaturized total chemical analysis systems: A novel concept for chemical sensing," *Sens. Actuators B Chem.*, vol. 1, no. 1, pp. 244–248, Jan. 1990.

[5] N. Meyne, W. Müller-Wichards, H. K. Trieu, and A. F. Jacob, "Quasi-lumped coplanar transmission-line sensors for broadband liquid characterization," in *2014 44th European Microwave Conference*, 2014, pp. 687–690.

[6] K. Grenier, D. Dubuc, T. Chen, F. Artis, T. Chretiennot, M. Poupot, and J. Fournie, "Recent Advances in Microwave-Based Dielectric Spectroscopy at the Cellular Level for Cancer Investigations," *IEEE Trans. Microw. Theory Tech.*, vol. 61, no. 5, pp. 2023–2030, May 2013.

[7] W. Chen, D. Dubuc, and K. Grenier, "Microwave dielectric spectroscopy of a single biological cell with improved sensitivity up to 40 GHz," in *IEEE MTT-S International Microwave Symposium*, 2015, pp. 1–3.

[8] Y. Ning, C. R. Multari, X. Luo, C. Palego, X. Cheng, J. C. M. Hwang, A. Denzi, C. Merla, F. Apollonio, and M. Liberti, "Broadband Electrical Detection of Individual Biological Cells," *IEEE Trans. Microw. Theory Tech.*, vol. 62, no. 9, pp. 1905–1911, Sep. 2014.

[9] X. Ma, X. Du, C. R. Multari, Y. Ning, X. Luo, V. Gholizadeh, C.Palego, X. Cheng, and J. C. M. Hwang, "Reproducible broadband measurement for cytoplasm capacitance of a biological cell," in *2016 IEEE MTT-S International Microwave Symposium (IMS)*, 2016, pp. 1–4.

[10] D. J. Rowe, A. Porch, D. A. Barrow, and C. J. Allender, "Microfluidic device for compositional analysis of solvent systems at microwave frequencies," *Sens. Actuators B Chem.*, vol. 169, pp. 213–221, Jul. 2012.

[11] D. J. Rowe, S. al-Malki, A. A. Abduljabar, A. Porch, D. A. Barrow, and C. J. Allender, "Improved Split-Ring Resonator for Microfluidic Sensing," *IEEE Trans. Microw. Theory Tech.*, vol. 62, no. 3, pp. 689–699, Mar. 2014.

[12] D. F. Williams, P. Corson, J. Sharma, H. Krishnaswamy, W. Tai, Z. George, D. Ricketts, P. Waston, E. Dacquay, and S. P. Voinigescu, "Calibration-Kit Design for Millimeter-Wave Silicon Integrated Circuits," *IEEE Trans. Microw. Theory Tech.*, vol. 61, no. 7, pp. 2685–2694, Jul. 2013.

[13] D. F. Williams and R. B. Marks, "LRM probe-tip calibrations using nonideal standards," *IEEE Trans. Microw. Theory Tech.*, vol. 43, no. 2, pp. 466–469, Feb. 1995.

[14] M. A. Pulido-Gaytán, J. A. Reynoso-Hernández, J. R. Loo-Yau, A. Z. Landa, and M. d C. Maya-Sánchez, "Generalized Theory of the Thru-Reflect-Match Calibration Technique," *IEEE Trans. Microw. Theory Tech.*, vol. 63, no. 5, pp. 1693–1699, May 2015.

[15] D. F. Williams and D. K. Walker, "Series-Resistor Calibration," in *50th ARFTG Conference Digest*, 1997, vol. 32, pp. 131–137.

[16] S. Padmanabhan, L. Dunleavy, J. E. Daniel, A. Rodriguez, and P. L. Kirby, "Broadband Space Conservative On-Wafer Network Analyzer Calibrations with More Complex Load and Thru Models," *IEEE Trans. Microw. Theory Tech.*, vol. 54, no. 9, pp. 3583–3593, Sep. 2006.

[17] R. B. Marks, "A multiline method of network analyzer calibration," *IEEE Trans. Microw. Theory Tech.*, vol. 39, no. 7, pp. 1205–1215, Jul. 1991.

[18] D. F. Williams, C. M. Wang, and U. Arz, "An optimal multiline TRL calibration algorithm," in *IEEE MTT-S International Microwave Symposium Digest*, 2003, vol. 3, pp. 1819–1822.

[19] A. Fraser, R. Gleason, and E. W. Strid, "GHz on-silicon-wafer probing calibration methods," in *Proceedings of the 1988 Bipolar Circuits and Technology Meeting*, 1988, pp. 154–157.

[20] D. F. Williams, J. C. M. Wang, and U. Arz, "An optimal vector-network-analyzer calibration algorithm," *IEEE Trans. Microw. Theory Tech.*, vol. 51, no. 12, pp. 2391–2401, Dec. 2003.

[21] S. Liu, I. Ocket, P. Barmuta, A. Lewandowski, D. Schreurs, and B. Nauwelaers, "Broadband dielectric spectroscopy calibration for microliter samples of biogenic liquid," in *2014 44th European Microwave Conference*, 2014, pp. 279–282.

[22] S. Liu, I. Ocket, P. Barmuta, T. Markovic, A. Lewandowski, D. Schreurs, and B. Nauwelaers, "Broadband dielectric spectroscopy calibration using calibration liquids with unknown permittivity," in *84th ARFTG Microwave Measurement Conference*, 2014, pp. 1–5.

[23] J. C. Booth, N. D. Orloff, J. Mateu, M. Janezic, M. Rinehart, and J. A. Beall, "Quantitative Permittivity Measurements of Nanoliter Liquid Volumes in Microfluidic Channels to 40 GHz," *IEEE Trans. Instrum. Meas.*, vol. 59, no. 12, pp. 3279–3288, Dec. 2010.

[24] R. B. Marks and D. F. Williams, "A general waveguide circuit theory," in *J. Res. Nat. Inst. Stand. Technol.*, vol. 97, no. 5, pp. 533–562, Sep./Oct. 1992.

[25] D. M. Pozar, "Microwave Engineering", 4th ed., John Wiley & Sons, Inc, 2011, pp. 48 – 56.

[26] D. Williams and R. Marks, "The Interpretation and Use of S-Parameters in Lossy Lines," in *36th ARFTG Conference Digest*, 1990, vol. 18, pp. 84–90.

[27] R. B. Marks and D. F. Williams, "Characteristic impedance determination using propagation constant measurement," *IEEE Microw. Guid. Wave Lett.*, vol. 1, no. 6, pp. 141–143, Jun. 1991.

[28] W. Heinrich, "Quasi-TEM description of MMIC coplanar lines including conductor loss effects," *IEEE Trans. Microw. Theory Tech.*, vol. 41, no. 1, Jan. 1993.

[29] K. LEVENBERG, "A METHOD FOR THE SOLUTION OF CERTAIN NON-LINEAR PROBLEMS IN LEAST SQUARES," *Q. Appl. Math.*, vol. 2, no. 2, pp. 164–168, 1944.

[30] S. Wittekoek, J. van der Werf, and R. A. George, "Phase Gratings as Waferstepper Alignment Marks for All Process Layers," in *Proc. SPIE*, 1985, vol. 538, pp. 24–31.

[31] J. Golden, H. Miller, D. Nawrocki and J. Ross, "Optimization of Bi-layer Lift-Off Resist Process," CS Mantech Technical Digest, 2009.

[32] N. D. Orloff, J. Mateu, A. Lewandowski, E. Rocas, J. King, D. Gu, X. Lu, C. Collado, I. Takeuchi, and J. C. Booth, "A Compact Variable-Temperature Broadband Series-Resistor Calibration," *IEEE Trans. Microw. Theory Tech.*, vol. 59, no. 1, pp. 188–195, Jan. 2011.

[33] H. Lorenz, M. Despont, N. Fahrni, N. LaBianca, P. Renaud, and P. Vettiger, "SU-8: a low-cost negative resist for MEMS," *J. Micromechanics Microengineering*, vol. 7, no. 3, pp. 121, 1997.

[34] J. C. McDonald and G. M. Whitesides, "Poly(dimethylsiloxane) as a Material for Fabricating Microfluidic Devices," *Acc. Chem. Res.*, vol. 35, no. 7, pp. 491–499, Jul. 2002.
[35] R. B. Marks, "Formulations of the Basic Vector Network Analyzer Error Model including Switch-Terms," in *50th ARFTG Conference Digest*, 1997, vol. 32, pp. 115–126.
[36] W. T. Weeks, L. L. Wu, M. F. McAllister, and A. Singh, "Resistive and inductive skin effect in rectangular conductors," *IBM J. Res. Develop.*, vol. 23, pp. 652-660, 1979.
[37] R. Buchner, J. Barthel, and J. Stauber, "The dielectric relaxation of water between 0°C and 35°C," *Chem. Phys. Lett.*, vol. 306, no. 1–2, pp. 57–63, Jun. 1999.
[38] C. A. E. Little, N. D. Orloff, I. E. Hanemann, C. J. Long, V. M. Bright, and J. C. Booth, "Modeling electrical double-layer effects for microfluidic impedance spectroscopy from 100 kHz to 110 GHz," *Lab Chip,* vol. 17, no. 15, pp. 2674–2681, July 2017.

Charles A. E. Little (Cully) received his B.S. in Physics from Appalachian State University in Boone, N.C. in 2008, after which he worked as a research assistant at Duke University as part of the Neutrino Group within the Physics Department. In 2013 he received his M.S. from the Mechanical Engineering Department of the University of Colorado, and is currently pursuing his Ph.D. in mechanical engineering, also at the University of Colorado. He has worked at the National Institute of Standards and Technology (NIST) in Boulder since beginning his master's work in 2010, developing fabrication techniques for microfluidics, with recent work concentrating on integrated microfluidic/microwave devices for measuring the electrical and magnetic properties of fluids.

Xiao Ma (S'15) received the B.S. degree in physics from Peking University, China in 2014. He is currently working towards his Ph.D. degree at Lehigh University. In the fall of 2016, he worked as a foreign guest researcher at NIST in Boulder on measurements and modeling for microwave microfluidic devices. Now his research interest includes biosensor, microwave measurement and liquid calibration. He is specialized in 3D electromagnetic simulation using finite element methods and microwave device characterization techniques.
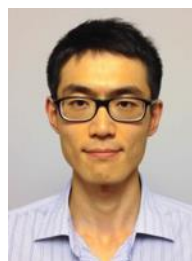
Christian J. Long, photograph and biography not available at the time of publication.

Isaac E. Hanemann，photograph and biography not available at the time of publication.

Nathan D. Orloff, received the B.S. (Hons.) and Ph.D. degrees in physics from the University of Maryland, College Park, MD, USA, in 2004 and 2010, respectively. His doctoral thesis involved the study and extraction of microwave properties of Ruddlesden-Popper ferroelectrics. In 2011, he was a Dean's Post-Doctoral Fellow with Prof. I. Riedel-Kruse at the Department of Bioengineering, Stanford University, Stanford, CA, USA. He joined the Materials Measurement Laboratory, National Institute of Standards and Technology, Gaithersburg, MD, USA, in 2013, as a Rice University Post-Doctoral Fellow with Prof. M. Pasquali. In 2014, Dr. Orloff joined the newly-formed Communications Technology Laboratory to lead the Microwave Materials Project. Dr. Orloff was a recipient of the 2004 Martin Monroe Undergraduate Research Award, the 2006 CMPS Award for Excellence as a Teaching Assistant, the 2010 Michael J. Pelczar Award for Excellence in Graduate Study, and the 2015 Communications Laboratory Distinguished Associate Award.

Song Liu received his Ph.D. degree in electrical engineering from KU Leuven, Belgium in 2016. His research interests include RF power amplifier design, microwave biomedical applications, VNA calibration, and material characterization. In 2014-2015, he spent six months in RF Technology Division, National Institute of Standards and Technology (NIST), Boulder, under the support of KU Leuven. He was one of the recipients of the ARFTG Roger Pollard student fellowship in 2013 and the MTT-S graduate fellowship in 2014.

Jordi Mateu received the Telecommunication Engineering and Ph.D. degrees from the Universitat Politècnica de Catalunya (UPC), Barcelona, in 1999 and 2003, respectively. Since 2007, he is with the Department of Signal Theory and Communications (TSC) at UPC, where he holds the position of Associate Professor,

and with Centre Tecnologic de Telecomunicacions de Catalunya (CTTC) as external Senior Research Associate. In addition to that he counts with over six years of experience outside the academia, as engineer, researcher and manager, namely Gillette (UK), Superconductor Technologies Inc., (CA), CTTC (Spain), MIT (MA), including over three years at NIST (CO).

James C. Booth, photograph and biography not available at the time of publication.
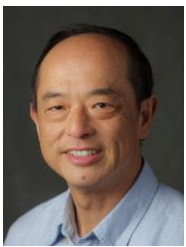
James C. M. Hwang (M'81–SM'82–F'94–LF'15) received the B.S. degree in physics from National Taiwan University, Taipei, Taiwan, and the M.S. and Ph.D. degrees in materials science and engineering from Cornell University, Ithaca, New York. Since 1988, he has been Professor of Electrical Engineering and Director of Compound Semiconductor Technology Laboratory at Lehigh University, Bethlehem, Pennsylvania. Prior to that, he spent twelve years at IBM, Bell Labs, GE, and GAIN. He cofounded GAIN and QED; the latter became a public company (IQE). He has worked on microwave materials, devices and circuits for four decades.